RECENT LOAD CALIBRATIONS EXPERIENCE

WITH THE YF-12 AIRPLANE

Jerald M. Jenkins and Albert E. Kuhl
Dryden Flight Research Center

SUMMARY

The results of recent experience using calibrated strain gages to measure wing loads on the YF-12A airplane are presented. Structural configurations relative to the thermal environment and resulting thermal stresses are discussed. A thermal calibration of the YF-12A is described to illustrate how contaminating thermal effects can be removed from loads equations. The relationship between ground load calibrations and flight measurements is examined for possible errors, and an analytical approach to accommodate such errors is presented.

INTRODUCTION

The measurement of structural loads is an important part of the flight test program on any new aircraft. In the past, these loads have been effectively measured by the use of calibrated strain gage systems (ref. 1). However, new supersonic and hypersonic aircraft often use complex delta-wing designs (refs. 2 to 4) and operate in higher temperature environments. This makes the measurement of structural loads more difficult. In addition to the fact that the delta-wing structure is harder to calibrate because of its structural complexities, the thermal effects present at the higher speeds (refs. 5 and 6) also cause contamination of the strain gage measurements necessary to deduce flight loads (ref. 7).

To obtain valid measurements of loads from aircraft operating in higher temperature environments, the use of thermally calibrated strain gage systems was investigated using the YF-12A aircraft as a typical delta-wing design (refs. 8 to 10). The errors which resulted from the induced thermal effects were determined. A simple computer model (ref. 11) was developed to predict strain patterns which would assist in placing strain gages and in developing load equations.

This report deals with the general philosophy used to calibrate the strain gage system and to determine the accuracy of the load equations when applied to a typical delta-wing configuration.

Physical quantities in this report are given in the International System of Units.

g	acceleration due to gravity, m-N/sec^2
L_A	wing loading due to aerodynamic forces, N or m-N
L_I	wing loading due to inertial forces, N or m-N
L_M	total measured wing loading, N or m-N
L_T	wing loading induced by thermal effects, N or m-N
T	temperature, K
t	time, min

STRUCTURAL CONFIGURATIONS

Supersonic and hypersonic wing designs (ref. 12) consider both aerodynamic and structural factors. The frequent use of the delta-wing shape reflects the obvious need for aerodynamic efficiency. However, structural considerations are more latent and require considerable explanation. Figure 1 shows a structural skeleton of the YF-12A airplane. The wing surfaces are built up of a beaded outer skin and a corrugated inner skin. These surfaces are supported by 28 closely-spaced spanwise beams and by four chordwise ribs. The wing beams are continuous through the fuselage. The engine nacelle is an integral part of the wing and the nacelle rings provide continuity between the inner and outer wing beams. A factor to be considered in the structural design of a supersonic wing is the presence of elevated structural temperatures and temperature gradients when operating in the higher Mach number range. Differential temperatures among structural elements, the effects of dissimilar materials, and nonlinear temperature distributions result in thermal stresses that can be very large.

There is little documented information about state-of-the-art methods for calculating thermal stresses in complex structures. This lack of information has probably led to avoidance design philosophies in which the designer configures the structure to avoid thermal stresses as much as possible. An example of avoidance design is illustrated in figure 2. In this case, the skin structure is corrugated to allow expansion in one direction. Skins of this type are generally attached to the substructure using a standoff-type clip which allows the expansion to be absorbed in an accordian-like manner. The standoff clips provide the structural continuity,

48

creating a heat shield effect. It is very likely that future designs will also include avoidance techniques similar to those used on the YF-12A airplane; however, while these designs reduce the magnitudes of thermal stresses, they do not eliminate them, as will be shown later.

THERMAL ENVIRONMENT

The primary problems arising from elevated structural temperatures concern the structure itself. There are two important factors which must be considered: the absolute magnitude of the temperature and the manner in which the temperature is distributed. The absolute magnitude of the temperature affects such things as the strength of the material, its stiffness, and the interactions between dissimilar materials. The temperature gradients and the nature of the gradients primarily affect the severity of the thermal stresses. Both of these factors influence measurements of flight loads using strain gages.

The isotherms shown in figure 3 illustrate how steady-state temperatures are distributed on the YF-12A airplane when cruising at Mach 3. Under these conditions maximum temperatures reach 589 K. The manner in which these temperatures increase is shown in figure 4 for different skin locations. It can be seen that, as the airplane increases speed to its Mach 3 cruise, the skin temperatures rise quickly to their steady-state values.

Although the skin areas generally reach steady-state temperatures quickly, this is not true of the substructure. The time history shown in figure 5 illustrates that the substructure spar cap and spar web are slow to reach steady-state temperature. In this case the airplane is at a Mach 3 cruise for 15 minutes before the substructure temperatures begin to stabilize. The same effect can be seen more graphically in figure 6 where the temperatures are plotted for four different time segments during a Mach 3 cruise flight. At the 8-minute time segment, the temperature gradients are large and the distribution of temperature is highly nonlinear. After about 32 minutes, the temperature reaches steady state. At that time, the gradients are not large and the nonlinearity is significantly reduced.

The nature of these gradients and the characteristics of nonlinearities have a large influence on the thermal stress patterns induced in the aircraft structure by the temperature field. Transient thermal stresses will be a major design concern in any future supersonic aircraft capable of speeds much above Mach 2. The presence of these thermal stresses can also cause errors in strain gage measurements of aerodynamic, inertial, or dynamic loads unless the thermal stresses are considered in the strain gage calibration procedures.

THERMAL STRESS

Two types of thermal stress result from the supersonic flight environment. The first type (ref. 13) results from the forces that arise in a system of mutually connected members as a result of their combined effect on one another. This may be caused by the use of materials having different coefficients of expansion, or it may

be caused by nonuniform temperatures in the bodies making up the system. A second type (ref. 13) results from nonlinearities in the temperature field or in the material properties of the body. This type of stress might occur if a single spar has a nonlinear temperature gradient through its depth. For example, consider the structural element in figure 7. If the temperature distribution shown is imposed on this skin/substructure element, thermal stresses arise due to the nonlinear nature of the temperature distribution. Thermal stresses in this case may be computed using elementary beam theory (ref. 14). The results of this type of thermal stress analysis are shown in figure 8.

The stress pattern in the skin reflects the heat sink effect of the substructure. Tensile stresses exist in the cooler areas near the substructure and compressive stresses exist in the hotter areas. A widely varying stress pattern is also present through the depth of the substructure. In this case, large tensile stresses exist in the web area, while the lower cap has compressive stresses. This demonstrates the need for a thorough analysis as part of any design or testing endeavor in which thermal stresses are a factor.

It is important to understand that the distribution of thermal stress shown in figure 8 is for a single instant in time. Thermal stresses are generally time-dependent and vary in direct relation to the manner in which the temperature field varies with time. Because the temperatures are constantly changing, thermal stresses in any one discrete element may vary from large compressive values to large tensile values during a flight.

The data presented in figure 9 were developed from laboratory heating tests on the YF-12A airplane. These ground heating tests determined the strain gage outputs due to the effects of heat alone. These outputs could then be put into the load equations, which are linear equations that relate several strain gage outputs to a set of calibration loads. From these equations the thermal load can be calculated. The transient behavior of strain gages can be seen indirectly in figure 9, which is a time history of the thermal errors for a set of shear, bending, and torsion equations. In this case, the thermal load is shown as a ratio with respect to a reference load. The reference load is the approximate wing loading under 1g flight conditions. The ratio values are used to provide a more meaningful measure of the relative magnitude of the thermal effects.

It was found that the outputs of the strain gages used in the shear and torque equations maximize near the time when the Mach 3 cruise begins. At that time, the value approaches half of the reference load. This correlates with the nonlinear distributions of temperature shown in figure 6. The nonlinearity of the temperature distribution has its greatest effect on the web thermal stresses which are primarily used to develop shear and torsion equations.

The time history of the bending equation is quite different. The value slowly builds to around 10 percent of the reference load near the end of the cruise. The bending gages, which are usually located on the caps or skins, were found to be more sensitive to the temperature rise than to the thermal stress levels.

The presence of thermal stresses of unknown magnitudes in the region where strain gages are located causes measurement errors, since the strain gages sense both aerodynamic forces and thermal effects. This problem is similar to the situation that arises when loads are measured during conventional subsonic maneuvering flight. In this case, the strain gages sense a combination of aerodynamic and inertial loads. The total measured load, L_M, is mathematically represented as:

$$L_M = L_A + L_I \tag{1}$$

where L_A is the total aerodynamic force and L_I is the total inertial force.

Since inertial loads can be calculated quite accurately if the mass characteristics of a wing are known, the aerodynamic load can be calculated by deducting the calculated inertial load from the total measured load:

$$L_A = L_M - L_I \tag{2}$$

This approach is commonly used to remove the inertial loads from flight data. The same type of relationship is valid for removing thermal effects for supersonic and hypersonic maneuvering flight. In this case the equation is:

$$L_A = L_M - L_T - L_I \tag{3}$$

where L_T is the fictitious load induced by the thermal effects. The philosophy of the correction is straightforward; however, implementing the correction is not so direct because determining the value of L_T is difficult. Frequently, the thermal load is large and must be determined with substantial accuracy. The ideal way to determine thermal effects would be to calculate the thermal stresses. Unfortunately, there is very little state-of-the-art information available about calculating thermal stresses in complex structures. The limited information (ref. 15) that is available indicates that large deviations exist between predicted and measured values. Precise calculations of thermal stresses also require a thorough and detailed definition of structural temperatures and such calculations would be awesome in size. Therefore, it does not appear that calculating the thermal stresses is a viable way to provide the load corrections unless considerable progress is made in calculative techniques.

A more direct approach to this problem uses a procedure known as a thermal calibration. In this procedure, the structure of the airplane is heated in a ground-based facility to obtain conditions identical to those experienced in flight. The objective of this procedure is to obtain the output from each of the strain gages that is due to heating effects only. In the laboratory environment, there are no aerodynamic or other external forces present (gravity excepted) to contaminate the determination of the thermal effects. This type of calibration was performed on the YF-12A airplane and the results are presented in reference 15. The thermal calibration procedure has proven to be feasible; however, the task of performing a thermal calibration is difficult. Duplicating an in-flight temperature time history for a complex airplane

structure is time consuming, costly, and technically complicated.

The facilities used to heat the airplane to obtain the thermal calibration are shown in figure 10. The airplane's surface temperatures were controlled by using thermocouples linked to a digital computer which commanded heating inputs from banks of radiant heat lamps. The surface of the airplane was divided into approximately 1000 zones which were independently controlled during the thermal calibration. The heating time histories of several flight profiles were simulated to provide corrections for several high Mach number conditions. The laboratory data were then used to correct the flight data.

Certain characteristics of thermal behavior should be known when thermal calibrations are necessary. Figure 11 shows temperature time histories of typical skin and web responses during three distinct phases of a flight: (A) increasing Mach number, (B) cruise at constant Mach number, and (C) decreasing Mach number. For the majority of the flight, the structure is in a state of changing temperature. The largest thermal stresses, and therefore the largest thermal corrections, occur during the transient portion of the flight, as indicated in figures 4 to 9. This means that when the temperatures are near steady state, as depicted in figure 12, the thermal corrections are at their smallest values. Early in the flight, the thermal component is large compared to the aerodynamic component of load. More possibility of error exists when the ratio of L_T/L_A is large because the correction value is large. When the ratio of L_T/L_A is small, such as for maneuver B, shown in figure 12, the errors present in the correction are also small and the aerodynamic component can be determined more accurately. Because of this, it is preferable to conduct load maneuvers near equilibrium conditions where the thermal gradients are small. However, sometimes special test requirements may be imposed that prevent the data from being obtained at the optimum thermal conditions. For example, if the data must be obtained for high airplane gross weights, this information cannot be obtained during the latter part of a flight. As a flight progresses, the constant-g wing loads decrease as the gross weight decreases due to fuel consumption, and this can affect the L_T/L_A ratio. Therefore, although it is preferable to get data late in the flight, there are instances in which exceptions must be made.

LOAD CALIBRATIONS

The traditional approach used to obtain wing loads data using calibrated strain gages has followed a sequence that includes: (1) locating strain gage bridges on pertinent structural members, (2) applying point loads to the wing in a grid pattern, (3) linearly relating the applied loads to the strain gage bridge outputs by means of a load equation, and (4) computing the equation error by using the strain gage bridge outputs in the equations, and then calculating the difference between the result and the known applied load. This approach has been used with great success for many years on high-aspect-ratio wings; however, the delta-wing shapes are not so amenable to this approach, and there is little additional information available regarding the calibration of delta-wing airplanes. Fortunately, recent experience has provided some additional information on the subject.

The basic problem arises from the fact that delta wings usually have multispar configurations with large chord dimensions relative to the span dimensions. With this configuration, a high degree of structural redundancy exists, which makes it difficult to determine how well a system can measure various load distributions. A study was conducted with two objectives: (1) to investigate a method to evaluate the accuracy of the load equations in deducing the true flight loads being measured and (2) to examine how well a simple computer structural model can be used to predict load response characteristics.

Mathematical Loadings

In order to develop a technique to evaluate the accuracy with which a load equation can compute various load distributions, it is necessary to identify a range of load distributions to serve as a standard. The three load distributions shown in figure 13 represent a reasonable cross section of expected loadings. Included are a loading with a forward center of pressure (typical of a subsonic load distribution), a loading with a central center of pressure (typical of a supersonic load distribution), and a loading with an aft center of pressure (typical of a loading induced by a large control surface deflection).

A method for interfacing the three mathematical loadings with the information developed from the load calibration is shown in figure 14. The load calibration provides influence coefficients and load equations. By subdividing the three mathematical loadings into local area loadings corresponding to the calibration load points, the strain gage bridge output can be calculated by multiplying the local area loading by the influence coefficient for that area. If this is done for all the local area loadings, and if all of the resulting outputs are summed, the result is the total output for each strain gage bridge due to the total mathematical wing loading. If these outputs are used appropriately in the load equations, a load may be calculated for comparison with the mathematically applied loading. This provides a functional check on how the load measuring system responds to varying load distributions.

This approach was used to examine the load calibration, and the subsequently developed load equations for the YF-12A airplane. A mathematical loading of 44,482 newtons was distributed over the surface of the wing according to the three load distributions described in references 16 to 18 and shown in figure 13. The procedures outlined in figure 14 were then used to calculate the loads from the superimposed strain gage outputs and the available load equations. The results are shown in figures 15 to 17.

As shown in figure 15, eight shear equations were checked using the procedure described. It was found that many of the equations calculated a load less than that mathematically applied. This implies a deficiency in the equations' ability to account for all the load on the surface. The worst cases occurred when the center of pressure was aft. Deficiencies of 20 percent or more were common for this condition.

The bending moment results (fig. 16) show a different trend. The greatest deficiency, between 5 and 10 percent, occurred in the central center-of-pressure case. In general, the bending moment equations seemed quite consistent and able to accommodate load variations well.

53

Six torsion equations are examined in figure 17. It is important to exercise caution when examining torsion data, since the reference axis location is arbitrary and this affects the magnitude of the results. It is also important to note that the vertical scales are different for the three cases. Although the equations provided reasonably accurate load calculations in two of the cases, a large discrepancy existed between the calculated load and the applied load for the aft center-of-pressure case.

There are two basic conclusions that can be drawn from this study: (1) There is still much that is not understood about calibrating low-aspect-ratio wings, and (2) computational procedures can be very helpful in selecting equations and in evaluating system errors.

Another interesting feature is apparent in figure 18, which shows the location of the calibration loads. The lengths of the vectors represent the magnitude of the loads. It is interesting to note that there is little correlation between the location of the large calibration loads and the location of the large flight loads depicted in figure 13. The magnitude of the calibration loads is usually a function of substructure bearing strength, and it does not necessarily correspond to the manner in which flight loads are distribued on the wing surface. This is a common condition, particularly on delta-wing structures.

Structural Computer Models

It is advantageous to know the nature of the structural response of various wing spars prior to developing a load calibration plan. A study was conducted to determine if a relatively simple structural model could be used to predict spar strain responses to load and to develop predicted influence coefficient plots of a general nature. Since the point of diminishing returns is quickly reached when the expense of modeling is considered, the study was limited to a simple structural model.

A bar element NASTRAN model of the wing of the YF-12A airplane was developed for this study. The ability of the model to predict strains along the root of the wing is shown in figures 19 and 20. In figure 19, the calculated and measured shear strains are shown at the wing root spars for loads applied to the wing at the locations and in the directions indicated by the arrows. It can be seen that the correlation between the measured shear strains and the strains calculated using the simple computer model is good. A similar comparison for bending strains is made in figure 20, and the correlation between the measured and predicted strains is also good.

In figures 21 and 22, influence coefficients have been calculated using the structural model, and they have been calculated from the laboratory load calibration data. The influence coefficients represent the strain that exists per unit of applied load. In the figures, the influence coefficient is plotted against the span on the basis of constant chord lines. The measured and calculated influence coefficients are compared in figure 21 for three different shear bridges located strategically along the wing root. The characteristic shapes of the measured and calculated curves are quite similar. In the first case the magnitude of the calculated data exceeds that of the measured data considerably; however, the general correlation is good. A similar comparison is shown in figure 22 for a bending bridge. The correlation for the bending bridges is also good and this plot is typical.

54

The results of this study indicate that considerable information can be gained from a simple structural computer model of a supersonic wing. This type of information is also extremely helpful in locating strain gages and in identifying potential strain gage combinations for use in load equations.

CONCLUDING REMARKS

Generally, wing configurations for supersonic, and even hypersonic airplanes, are low-aspect-ratio structures, with delta-wing shapes occurring most frequently. Present design trends configure the structure to avoid large thermal stresses. However, since there is no practical way to eliminate thermal stresses entirely, they must be considered in the design, testing, and operation of supersonic and hypersonic airplanes.

All aircraft which operate in the high supersonic and hypersonic speed ranges experience the effects of aerodynamic heating. Both high temperatures and large thermal gradients affect the validity of load measurements using calibrated strain gages. Structural temperature levels may even become high enough to alter spar stiffness, which could result in load path changes that might subsequently invalidate the wing strain gage calibration. Nonuniform temperature distributions also induce thermal stresses which can be very large and which can contaminate flight measurements of loads using strain gages.

Thermal effects which prevent valid high Mach number strain gage data from being obtained can be determined by thermally calibrating supersonic airplanes. Therefore, a ground laboratory heating simulation is a necessary part of the flight test program if valid loads data are to be obtained. The magnitudes of thermally induced loads vary in the supersonic environment, but they are large enough to require consideration in all cases.

A study to examine the adaptability of a set of load equations selected solely on the basis of the load calibrations revealed that discrepancies can exist if the loads to be measured are not considered in the overall selection process. The study also indicated that a relatively simple structural computer model can be very useful in predicting strain response to external loads with relatively good accuracy. This capability provides considerable foresight in locating strain gages and in identifying possible strain gage combinations for use in load equations.

REFERENCES

1. Skopinski, T. H.; Aiken, William S., Jr.; and Huston, Wilber B.: Calibration of Strain-Gage Installations in Aircraft Structures for the Measurement of Flight Loads. NACA Rept. 1178, 1954.

2. Jenkins, Jerald M.; DeAngelis, V. Michael; Friend, Edward L.; and Monaghan, Richard C.: Flight Measurements of Canard Loads, Canard Buffeting, and Elevon and Wing-Tip Hinge Moments on the XB-70 Aircraft Including Comparisons with Predictions. NASA TN D-5359, 1969.

3. Rich, Ben R.: The F-12 Series Aircraft Aerodynamic and Thermodynamic Design in Retrospect. AIAA Paper 73-820, Aug. 1973.

4. Ripley, E. L.: Structural Tests for the Supersonic Transport Aircraft. Technical Report 70121, Royal Aircraft Establishment (Farnborough, Hants., England), July 1970.

5. Quinn, Robert D.; and Olinger, Frank V.: Flight Temperatures and Thermal Simulation Requirements. NASA YF-12 Flight Loads Program. NASA TM X-3061, 1974, pp. 145-183.

6. Olinger, Frank V.; Sefic, Walter J.; and Rosecrans, Richard J.: Laboratory Heating Tests of the Airplane. NASA YF-12 Flight Loads Program. NASA TM X-3061, 1974, pp. 207-257.

7. Jenkins, Jerald M.: Some Views on the Use of Strain Gages for Flight Loads Measurements on Future High Performance Aircraft. Proceedings of Western Regional Strain Gage Committee, —1969 Spring Meeting, Philip O. Vulliet, ed., pp. 1-2. (Available from Soc. for Exp. Stress Analysis, 21 Bridge Sq., Westport, Conn. 06880.)

8. Fields, Roger A.: Strain Gage Measurement of Flight Loads at Elevated Temperature. NASA YF-12 Flight Loads Program. NASA TM X-3061, 1974, pp. 259-302.

9. Sefic, Walter J.; and Reardon, Lawrence F.: Loads Calibration of the Airplane. NASA YF-12 Flight Loads Program. NASA TM X-3061, 1974, pp. 61-107.

10. Jenkins, Jerald M.; and Kuhl, Albert E.: Summary of Recent Results Pertaining to Strain Gage Load Measurement Technology on High Speed Aircraft. NASA YF-12 Flight Loads Program. NASA TM X-3061, 1974, pp. 303-323.

11. Jenkins, Jerald M.; Kuhl, Albert E.; and Carter, Alan L.: The Use of a Simplified Structural Model as an Aid in the Strain Gage Calibration of a Complex Wing. NASA TM-56046, 1977.

12. Plank, P. P.; and Pennings, F. A.: Hypersonic Wing Test Structure Design, Analysis, and Fabrication. NASA CR-127490, 1973.

56

13. Fridman, Ya. B., ed.: Strength and Deformation in Nonuniform Temperature Fields. Authorized translation from the Russian, Consultants Bureau, New York, 1964.

14. Boley, Bruno A.; and Weiner, Jerome H.: Theory of Thermal Stresses. New York. John Wiley & Sons, Inc., 1962.

15. Carter, Alan L.: Assessment of Recent Loads Analysis Methods as Applied to a Mach 3 Cruise Airplane. NASA YF-12 Flight Loads Program. NASA TM X-3061, 1974, pp. 625-645.

16. Allen, H. Julian: General Theory of Airfoil Sections Having Arbitrary Shape or Pressure Distribution. NACA Rept. 833, 1945.

17. DeYoung, John; and Harper, Charles W.: Theoretical Symmetric Span Loading at Subsonic Speeds for Wings Having Arbitrary Plan Form. NACA Rept. 921, 1948.

18. Tucker, Warren A.; and Nelson, Robert L.: Theoretical Characteristics in Supersonic Flow of Two Types of Control Surfaces on Triangular Wings. NACA Rept. 939, 1949.
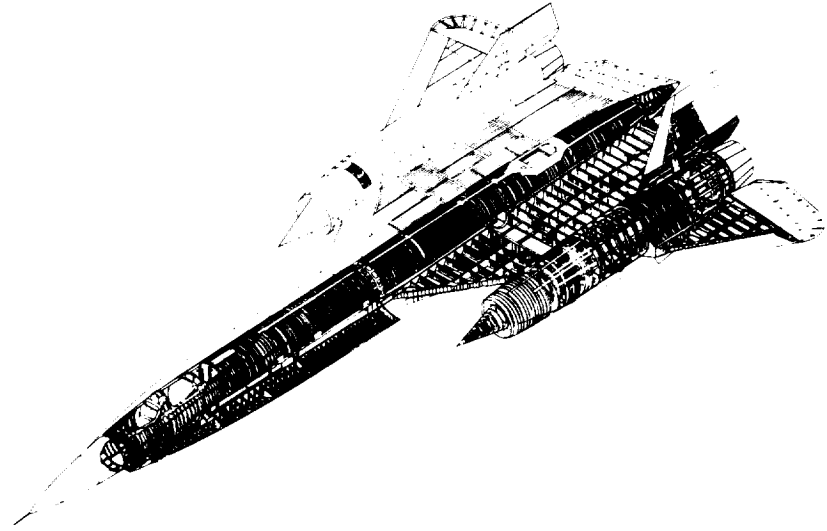
Figure 1.—Structural skeleton of a complex delta-wing aircraft.
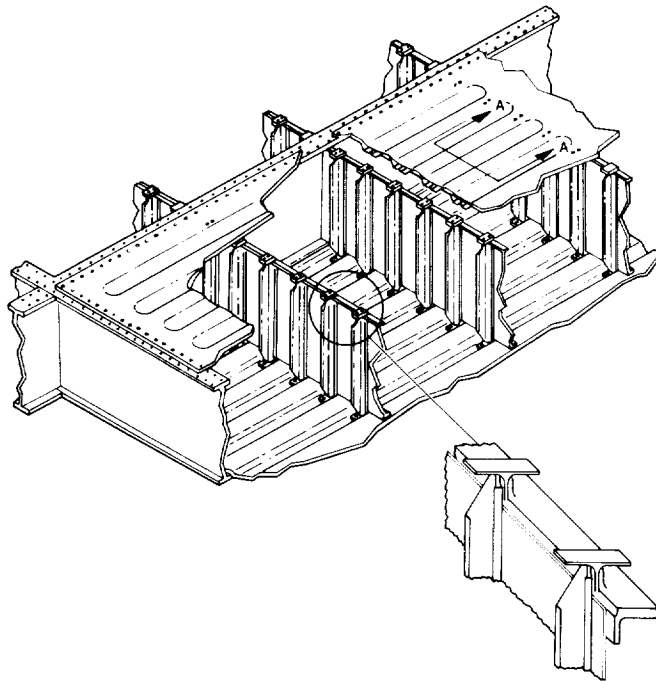
Figure 2.—Wing design used to minimize thermal stress.
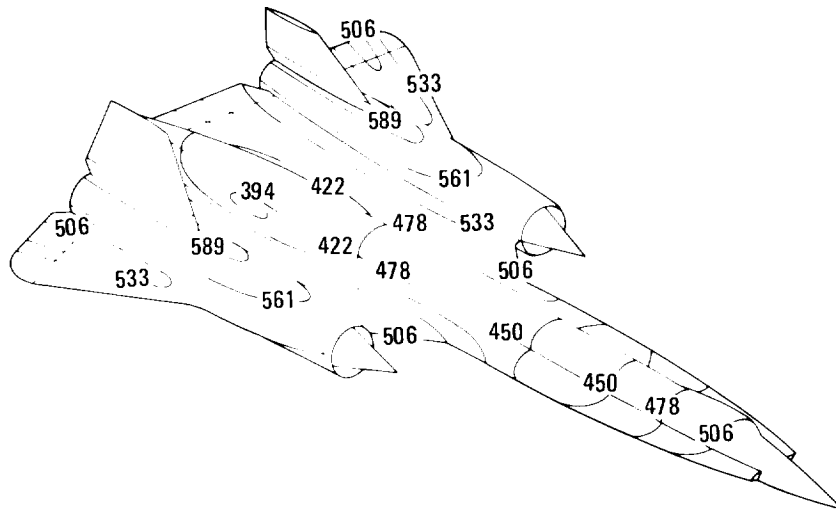
Figure 3.—Surface temperatures at high-Mach-number cruise condition.
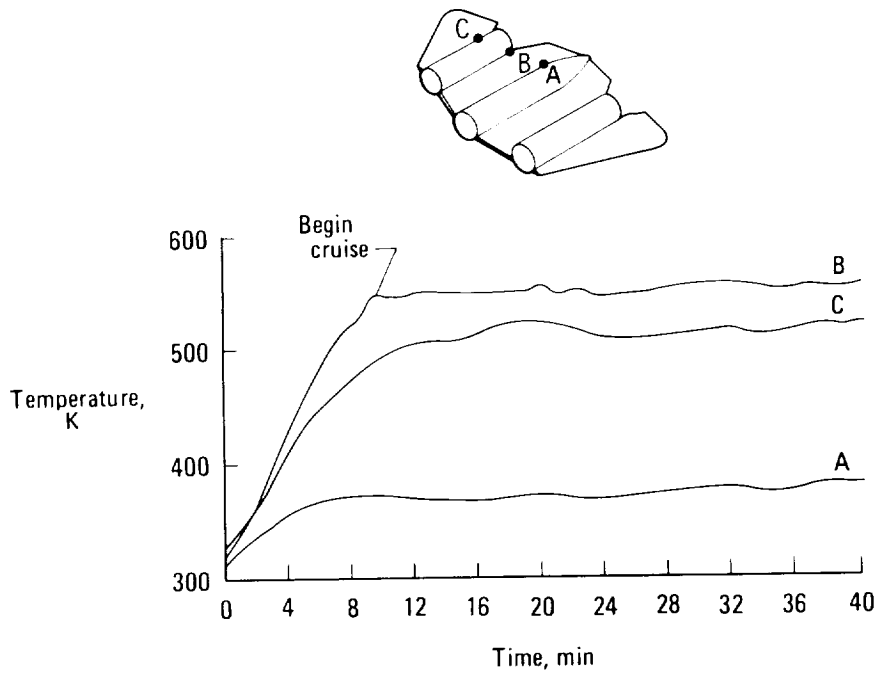
Figure 4.—Time history of typical wing skin surface temperatures.
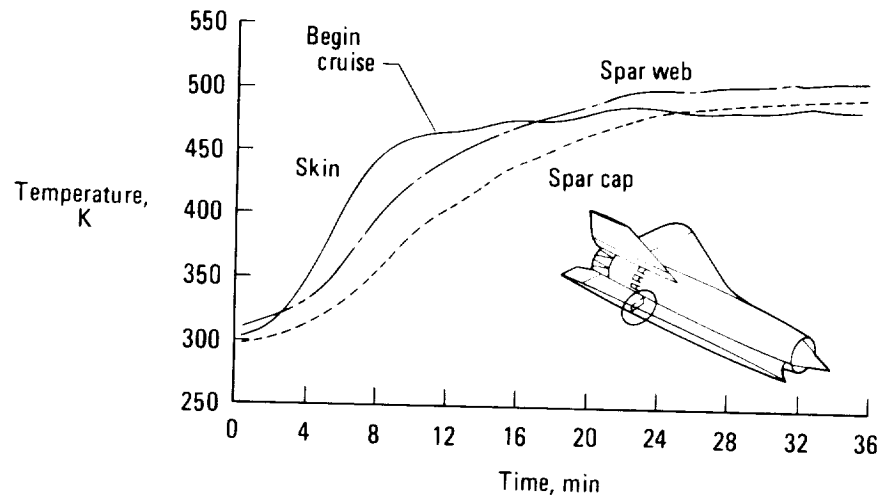
Figure 5.—Time history of typical wing spar temperature distribution.
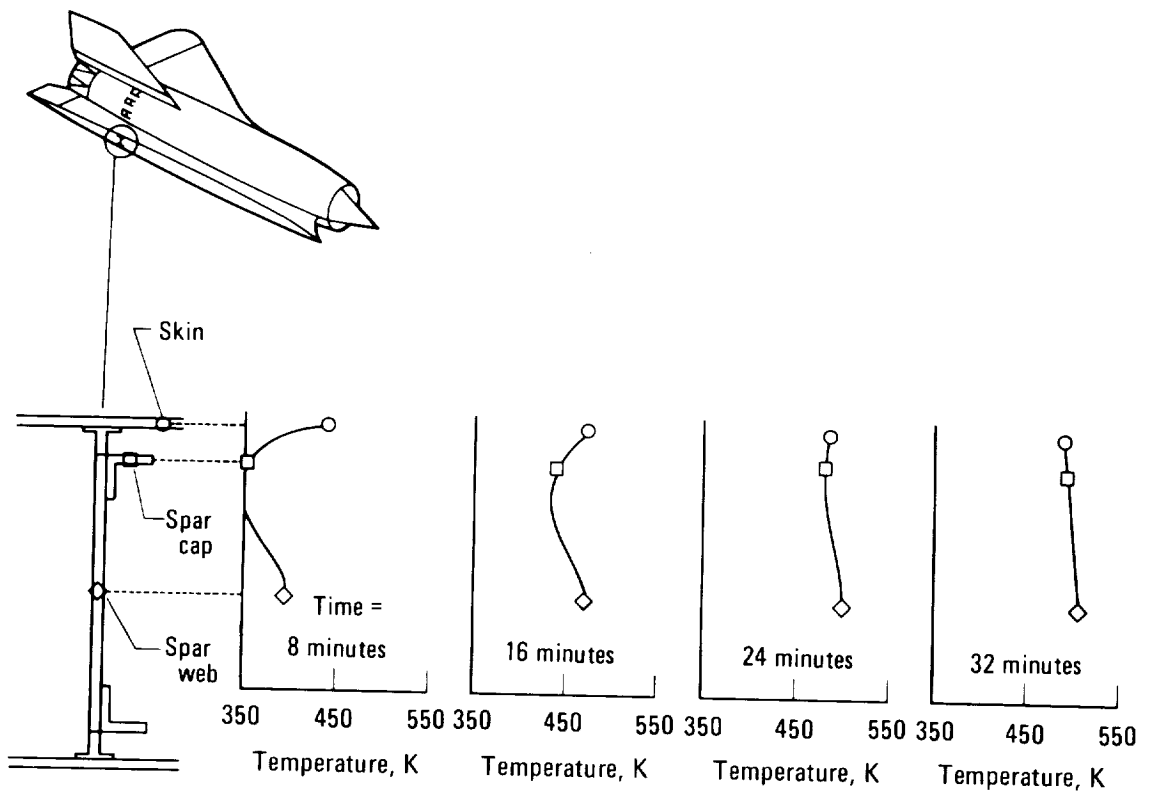
Figure 6.—Distribution of typical temperatures in wing spar.
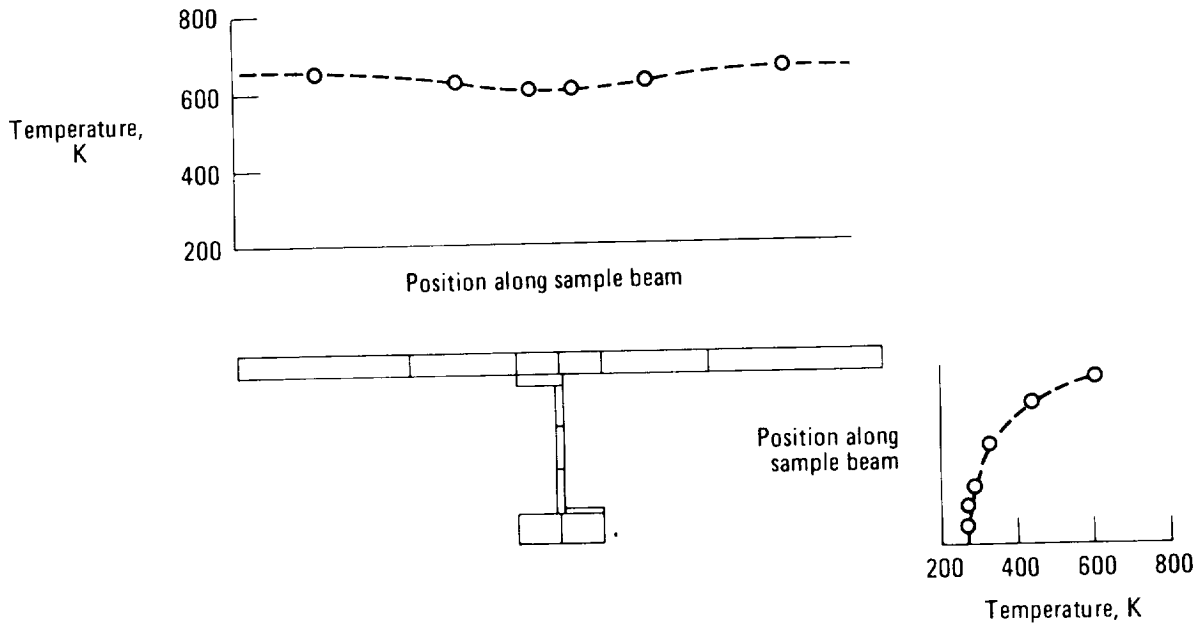
Figure 7.—Temperature distribution for analysis of sample beam.
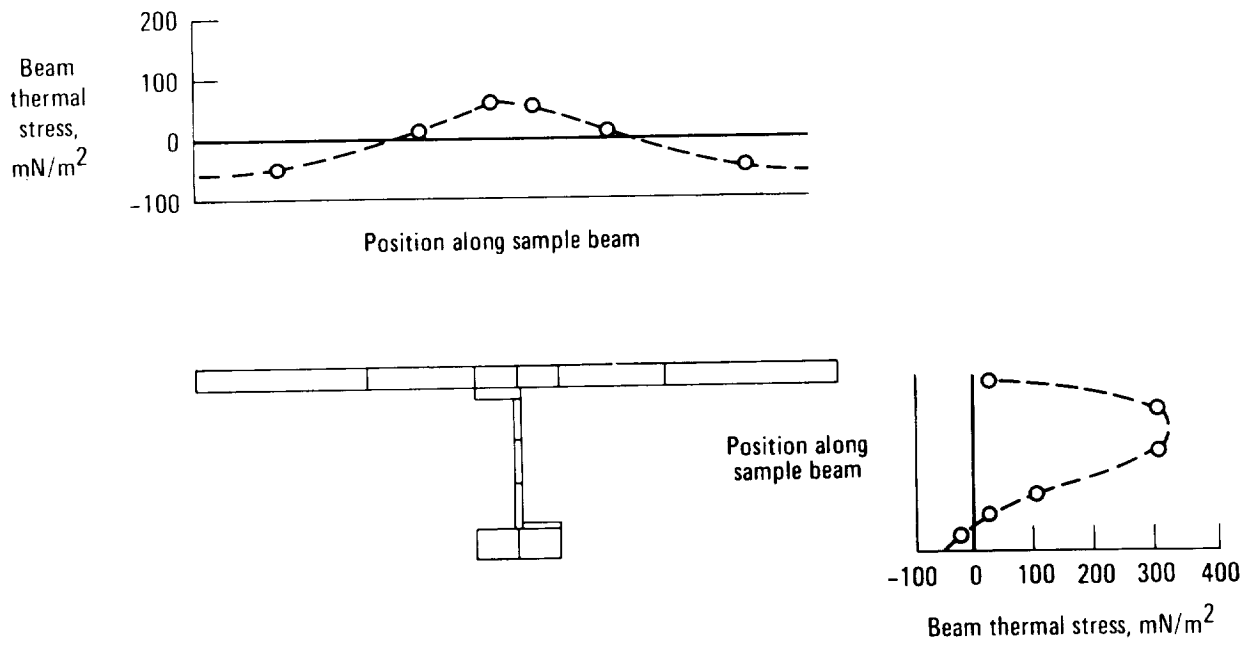
Figure 8.—Thermal stress distribution for analysis of sample beam.

61
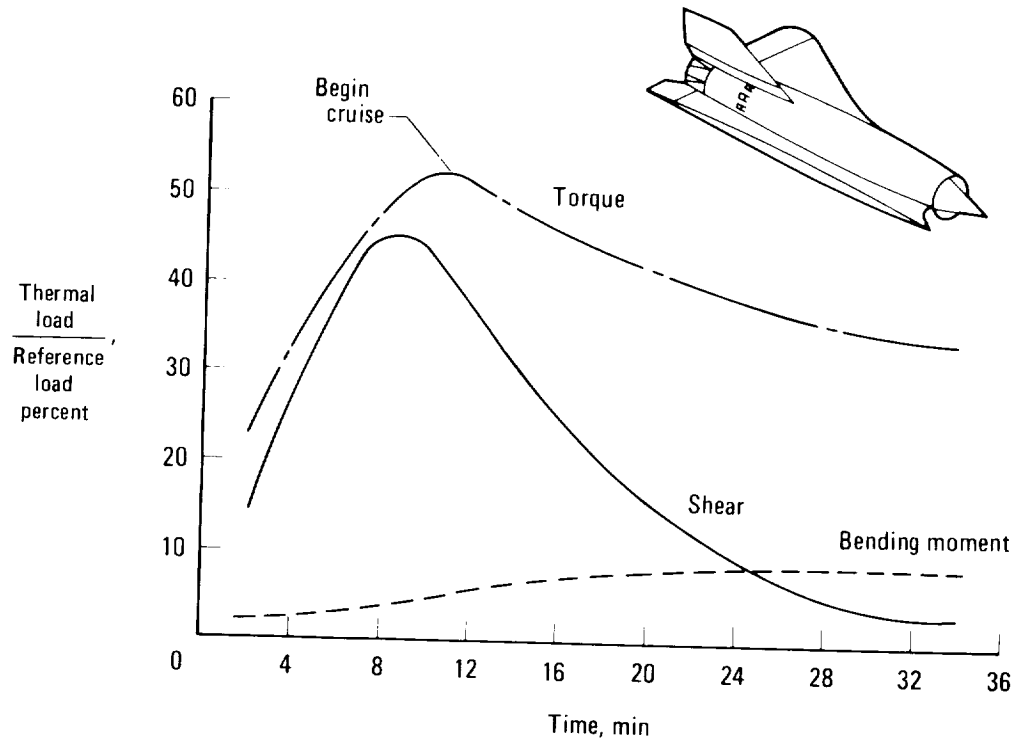
Figure 9.—Thermal effects on strain gage load equations.
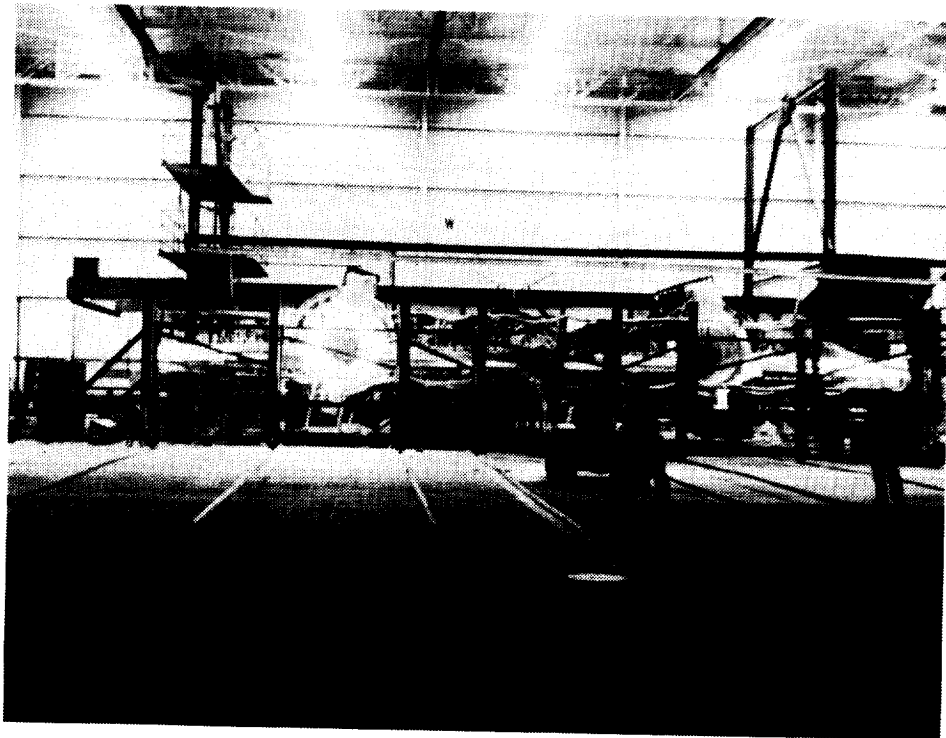
Figure 10.—Radiant heating of the airplane during the thermal calibration.

A Climb (increasing
Mach number)
B Cruise (constant
Mach number)
C Descent (decreasing
Mach number)
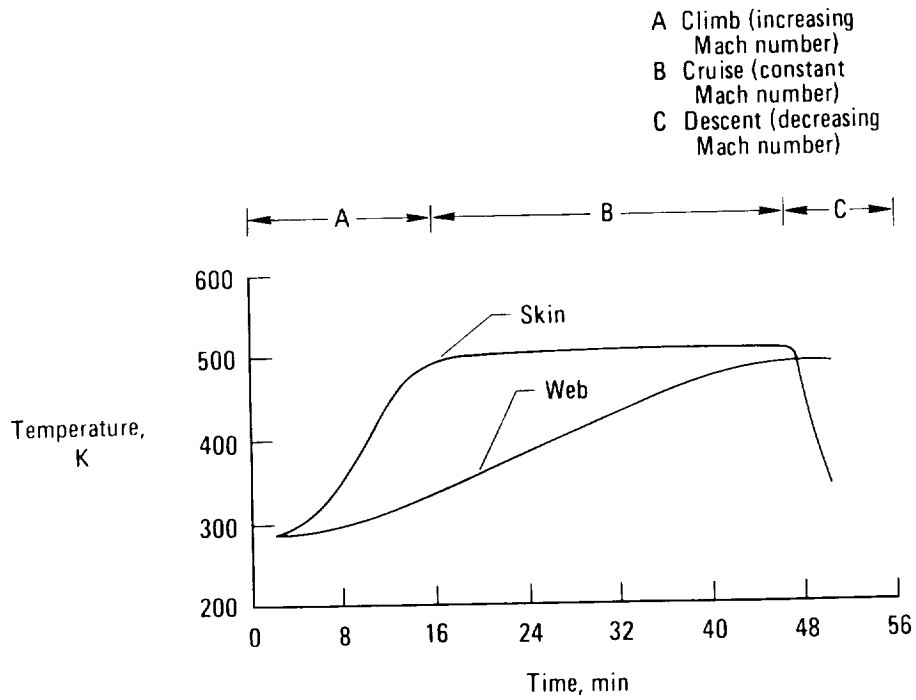
Figure 11.—Thermal profile of a supersonic flight.
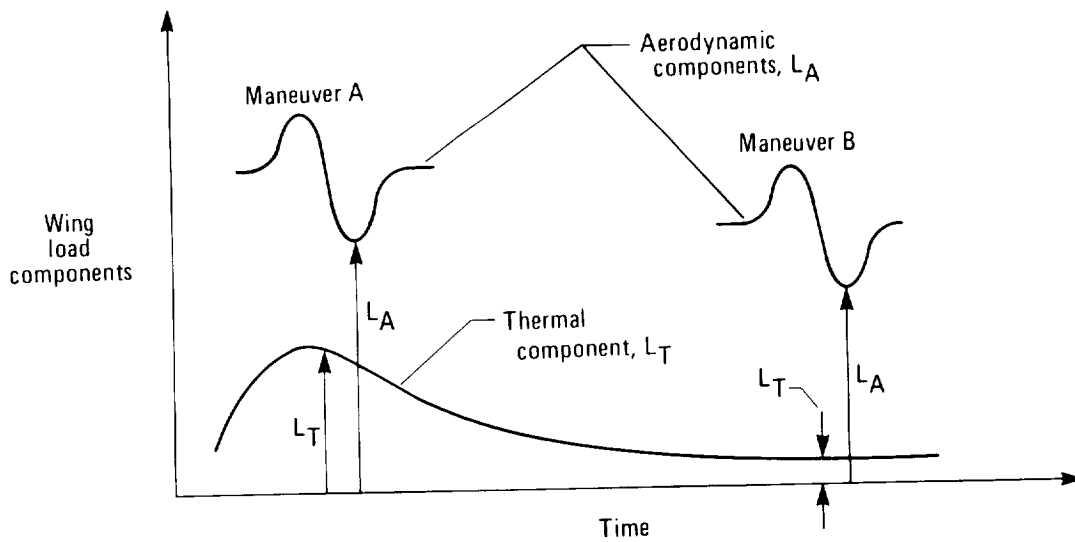
Figure 12.—Aerodynamic and thermal components of load relative to flight profile.

63

Forward center of pressure

Central center of pressure

Aft center of pressure
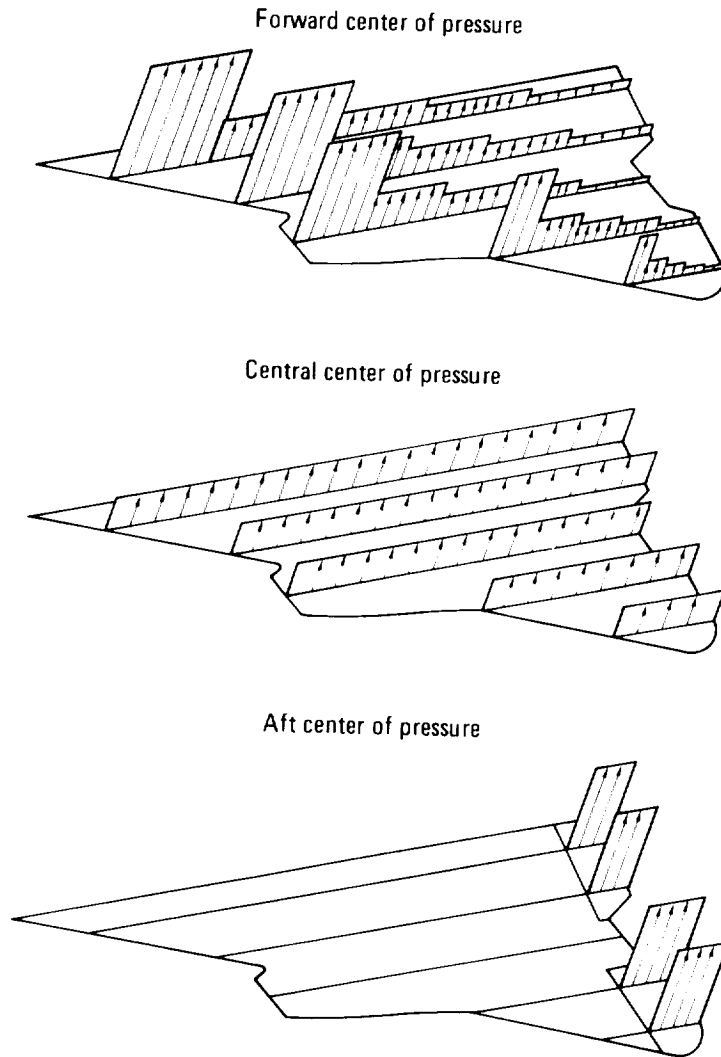
Figure 13.—Distribution of mathematically applied loads.
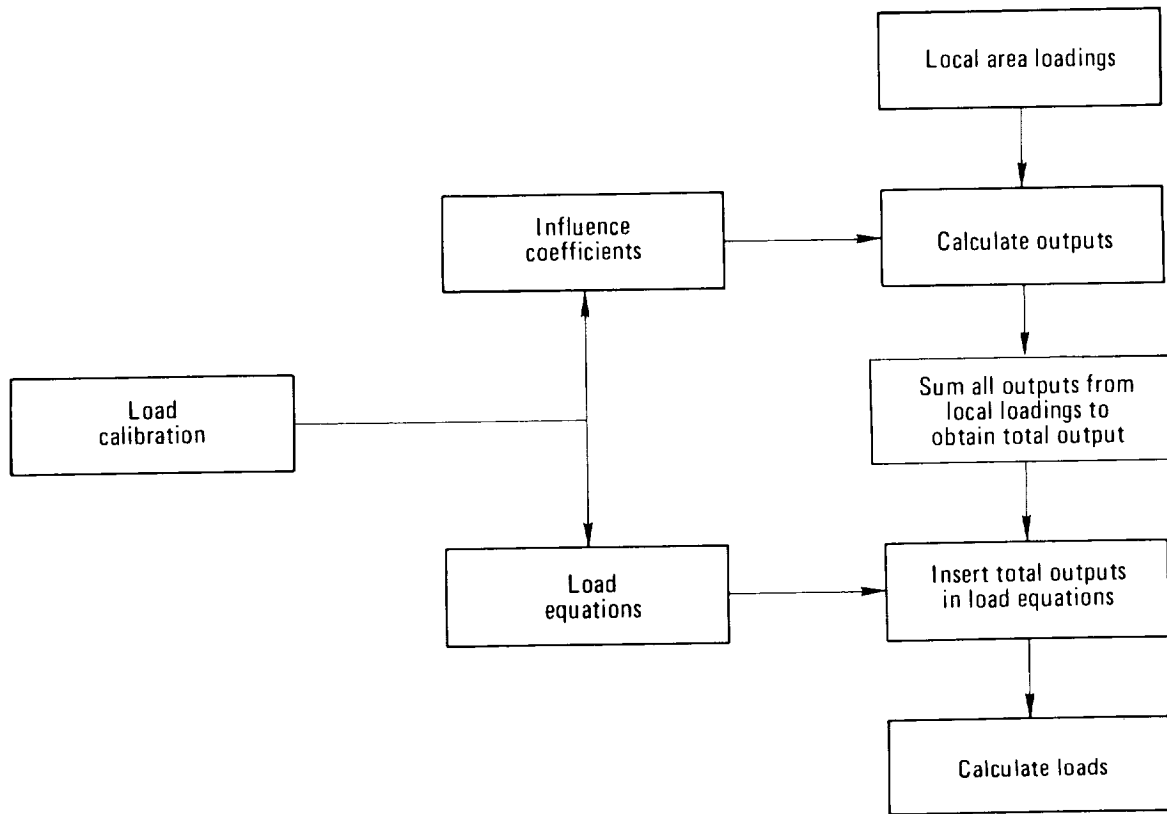
Figure 14.—Schematic showing computation of mathematically applied loads.
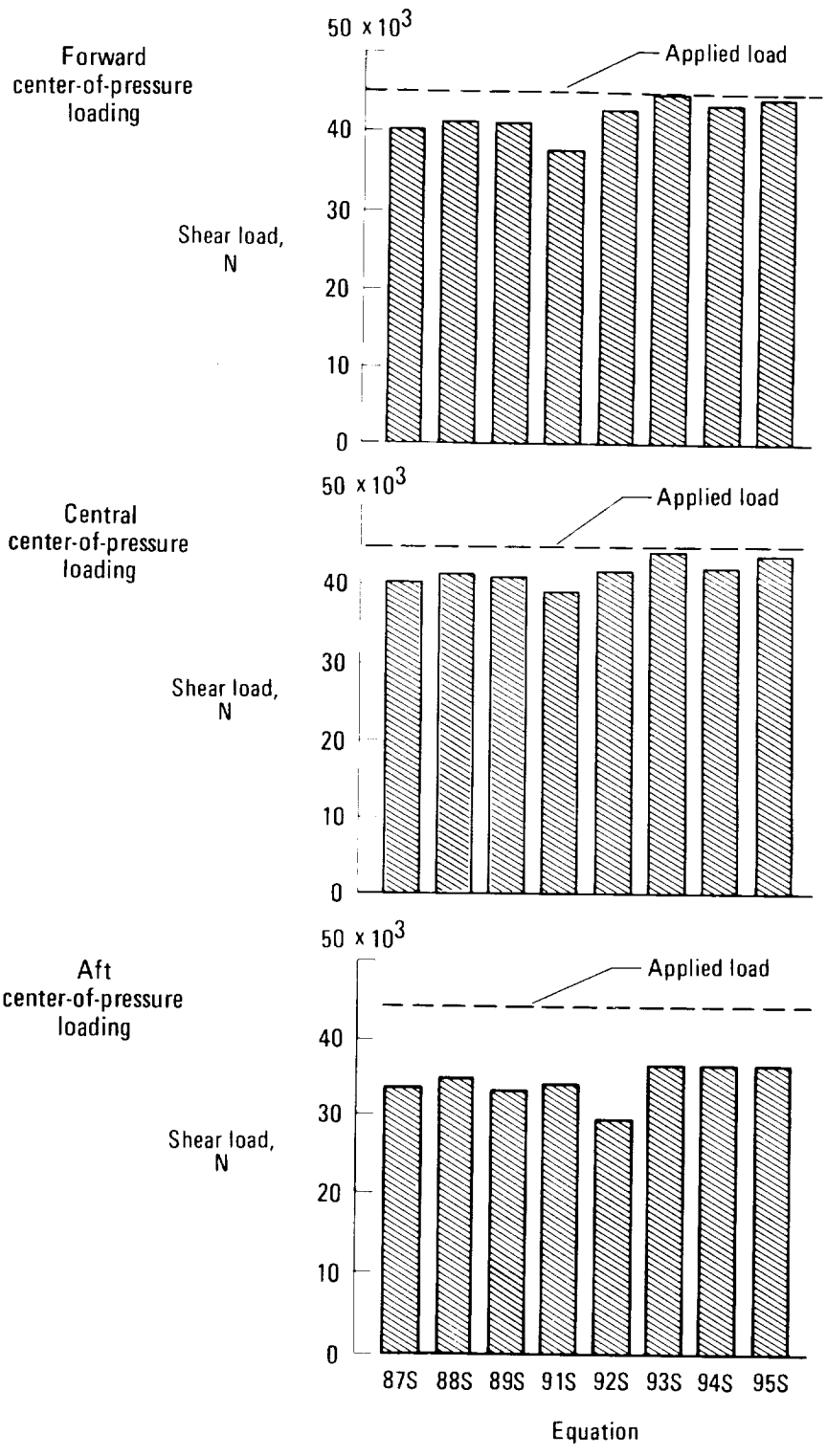
Figure 15.—Comparison of calculated and mathematically applied shear loads.
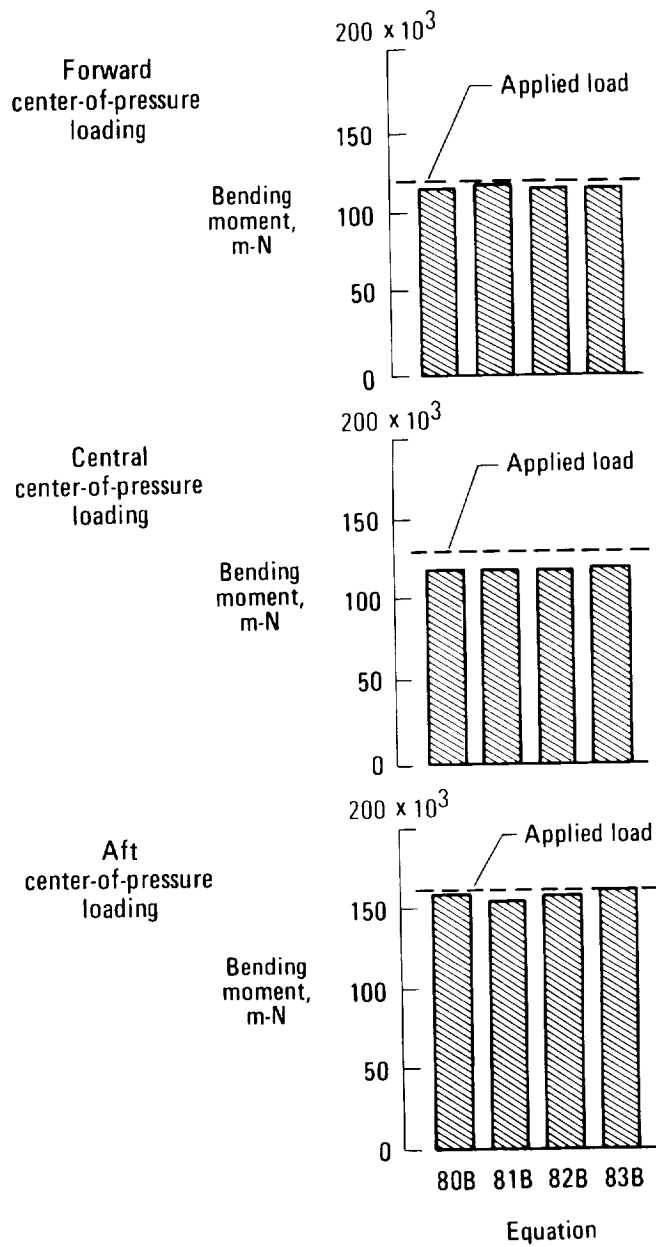
Figure 16.—Comparison of calculated and mathematically applied bending moments.
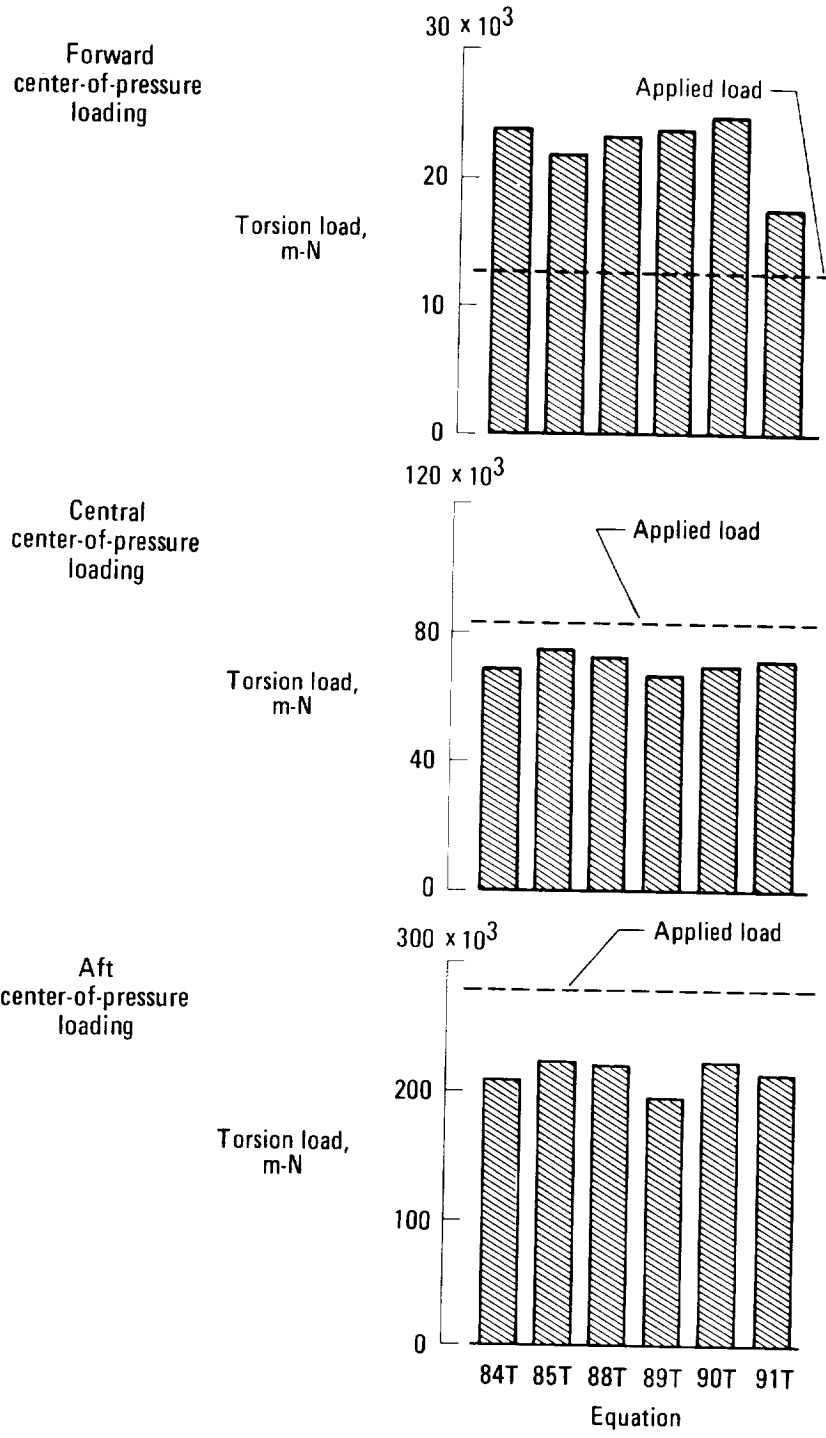
Figure 17.—Comparison of calculated and mathematically applied torsion loads.
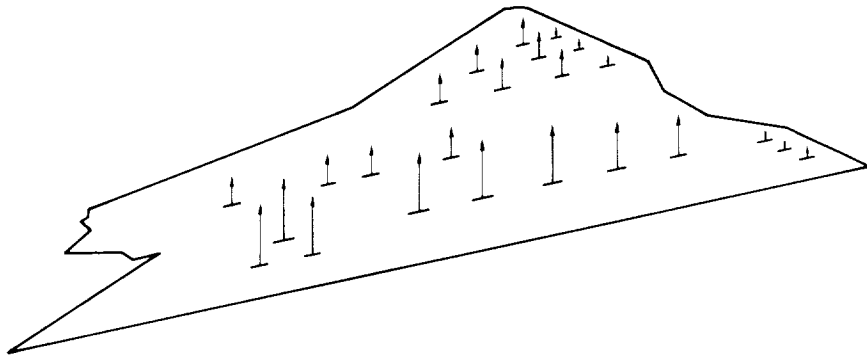
Figure 18.—Location and relative magnitude of loads applied during load calibration.
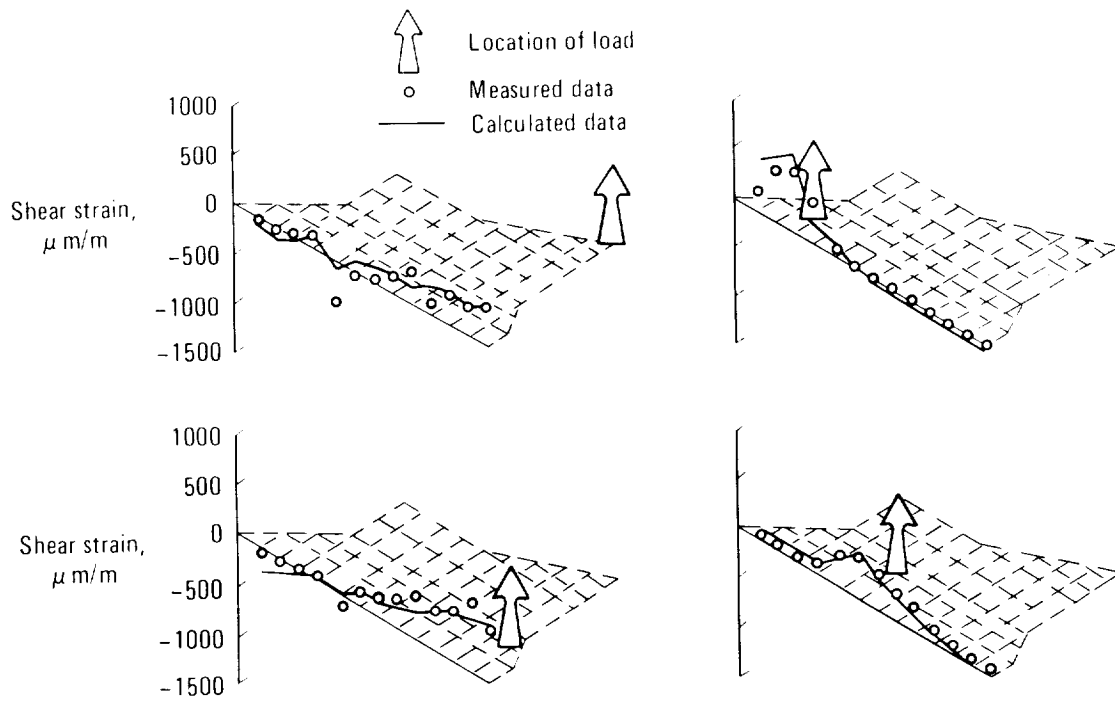
Figure 19.—Comparison of measured and calculated shear strains for several discrete loads.
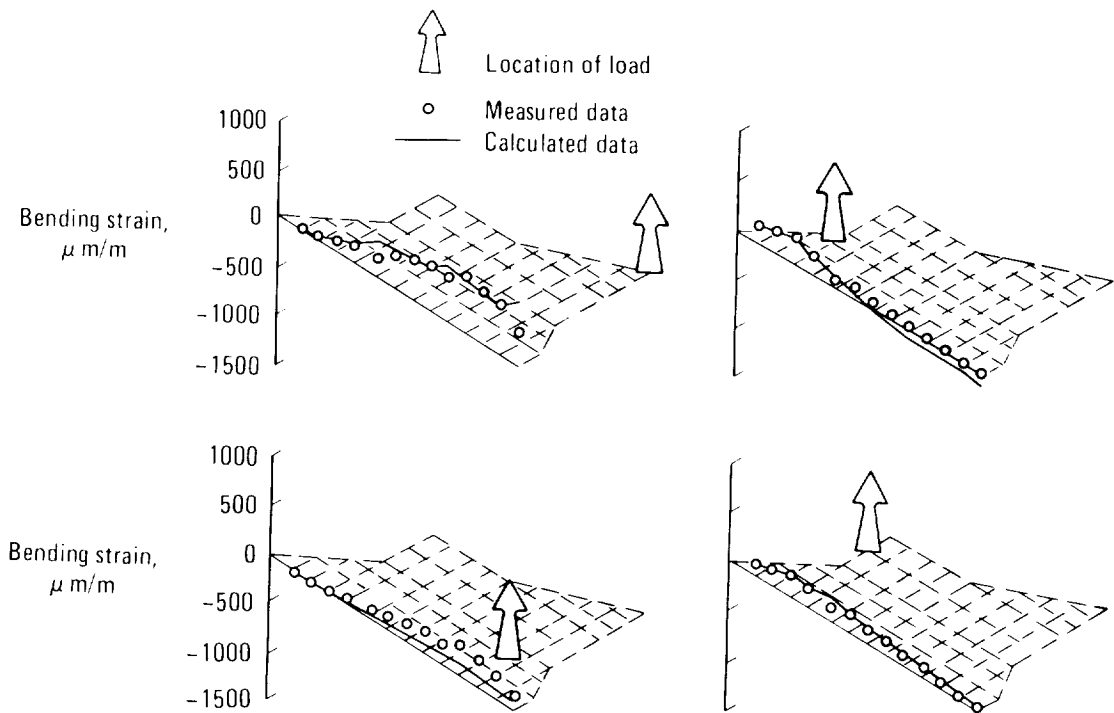
Figure 20.—Comparison of measured and calculated bending strains for several discrete loads.

70
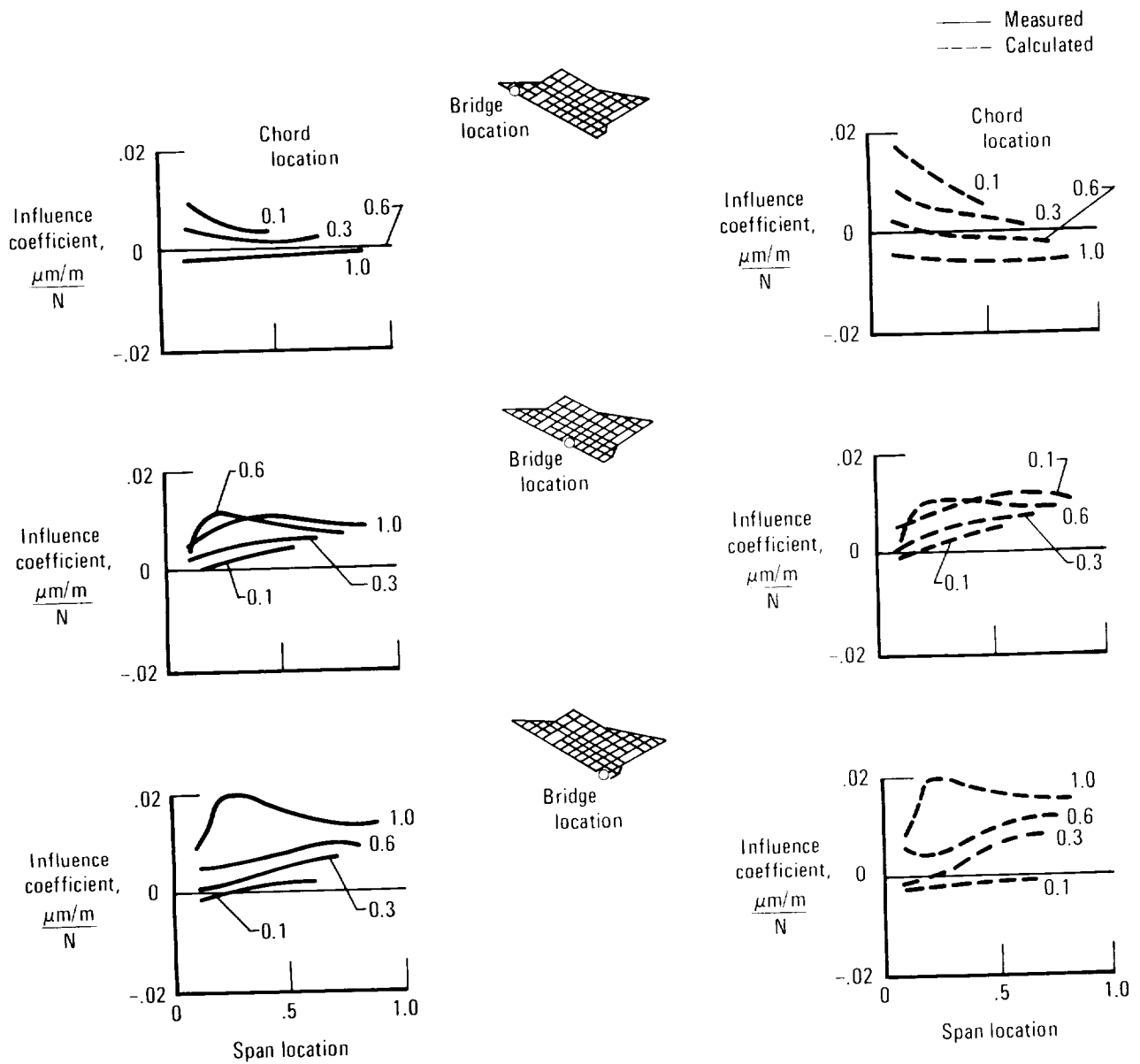
Figure 21.—Comparison of measured and calculated influence coefficient plots for shear strain.
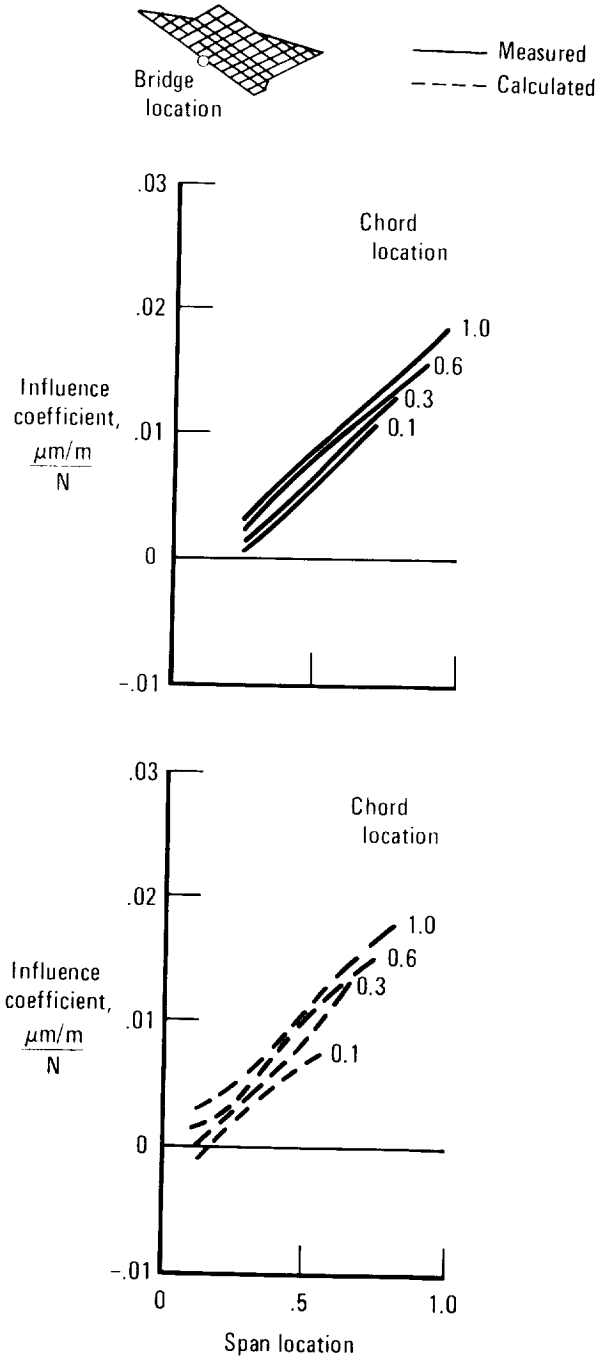
Figure 22.—Comparison of measured and calculated influence
coefficient plots for bending strain.